The HKU Scholars Hub   The University of Hong Kong   香港大學學術庫

Title	**Three-dimensional strain state and spacer thickness-dependent properties of epitaxial Pr0.7Sr0.3MnO3/La0.5Ca0.5MnO3/Pr0.7Sr0.3MnO3 trilayer structure**
Author(s)	**Wang, HO; Zhang, J; Jia, QJ; Xu, F; Tan, WS; Huo, DX; Gao, J**
Citation	**Journal of Applied Physics, 2014, v. 115 n. 23, article no. 233911, p. 233911:1-7**
Issued Date	**2014**
URL	**http://hdl.handle.net/10722/203325**
Rights	**Journal of Applied Physics. Copyright © American Institute of Physics**

Haiou Wang, Jie Zhang, Quanjie Jia, Feng Xu, Weishi Tan, Dexuan Huo, and Ju Gao
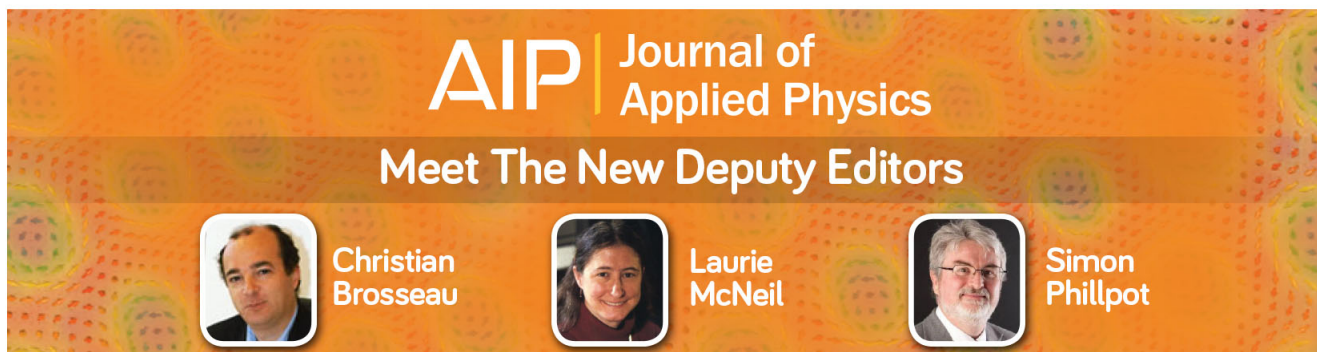

Articles you may be interested in

Enhanced Jahn-Teller response induced by low-dose 10MeV I+ irradiation of La0.7Ca0.3MnO3−δ films
Appl. Phys. Lett. **104**, 212404 (2014); 10.1063/1.4875385

Colossal anisotropic resistivity and oriented magnetic domains in strained La0.325Pr0.3Ca0.375MnO3 films
Appl. Phys. Lett. **104**, 203501 (2014); 10.1063/1.4878557

Magnetic proximity effect in Pr0.5Ca0.5MnO3/La0.7Sr0.3MnO3 bilayered films
Low Temp. Phys. **38**, 41 (2012); 10.1063/1.3677235

Influence of structural disorder on magnetic and transport properties of (La 0.7 Sr 0.3) 0.5 (Pr 0.65 Ca 0.35) 0.5 MnO 3 films
Low Temp. Phys. **31**, 161 (2005); 10.1063/1.1820566

Strain-stabilized charge ordering and magnetorelaxor behaviors in Cr-doped Pr 0.5 Ca 0.5 MnO 3 epitaxial thin films
Appl. Phys. Lett. **78**, 3505 (2001); 10.1063/1.1376146

Three-dimensional strain state and spacer thickness-dependent properties of epitaxial $Pr_{0.7}Sr_{0.3}MnO_3$/$La_{0.5}Ca_{0.5}MnO_3$/$Pr_{0.7}Sr_{0.3}MnO_3$ trilayer structure

Haiou Wang,[1,2,a)] Jie Zhang,[3] Quanjie Jia,[3] Feng Xu,[4] Weishi Tan,[2,a)] Dexuan Huo,[1] and Ju Gao[5]

[1]Institude of Material Physics, Hangzhou Dianzi University, Hangzhou, Zhejiang 310018, China
[2]Key Laboratory of Soft Chemistry and Functional Materials, Ministry of Education, Department of Applied Physics, Nanjing University of Science and Technology, Nanjing 210094, China
[3]Institute of High Energy Physics, The Chinese Academy of Sciences, Beijing 100039, China
[4]Department of Material Science and Engineering, Nanjing University of Science and Technology, Nanjing 210094, China
[5]Department of Physics, The University of Hong Kong, Hong Kong, China

Epitaxial colossal magnetoresistive trilayer structures consisting of ferromagnetic metallic $Pr_{0.7}Sr_{0.3}MnO_3$ (PSMO) and antiferromagnetic insulator $La_{0.5}Ca_{0.5}MnO_3$ (LCMO) were fabricated on (001)-oriented single crystal MgO substrates using pulsed laser deposition technique. The evolution of three-dimensional strain states and electrical and magnetic transport properties of PSMO/LCMO/PSMO trilayers have been studied as a function of LCMO spacer thickness and lattice strain. When the thickness of LCMO spacer is 6 nm, lattice strain in the trilayer begins to be relaxed. Furthermore, trilayers with thickness of LCMO spacer up to 36 nm are not fully strain relaxation. The unit cell volume of the films is not conserved and exhibits the variation with LCMO layer thickness. Strain relaxation states are determined by bulk strain (ε_B) and Jahn–Teller (ε_{JT}) strain together. The electrical and magnetic transport properties, including metal-insulator transition temperatures T_{MI} and saturation magnetization M_S, also show systematic variations with respect to LCMO layer thickness. © 2014 AIP Publishing LLC.
[http://dx.doi.org/10.1063/1.4884995]

I. INTRODUCTION

Since the discovery of colossal magnetoresistance (CMR) effect in epitaxial thin films of doped perovskite manganites,[1] there has been a renewed interest in these materials due to their potential application in magnetoelectronic devices.[2] The type of magnetic film, such as sandwich structure and double-layered structure of various systems, is extremely rich, including magnetic metal/nonmagnetic metal, magnetic metal/nonmagnetic insulator, ferromagnetic (FM)/antiferromagnetic (AFM) layer, etc.[3] The interface of manganite multilayers will play an important role in determining physical properties of multilayer because magnetic coupling occurs at the interface. On the other hand, the physical properties of manganites multilayer such as Curie temperature, Metal-insulators translation temperature, and low field magnetoresistance can also be tuned by changing thickness of the constituent element layer.[4–7] Experimental results on $La_{0.67}Sr_{0.33}MnO_3$ films[8] indicated that lattice distortion has the same influence on physical properties as that of sublayer thickness. The enhancement of lattice distortion will decrease saturation magnetization and alter temperature-dependent magnetoresistance. CMR effect in epitaxial $La_{0.625}Ca_{0.375}MnO_3$ films strongly increases with decrease of film thickness and strain relaxation degree, confirming the important role of lattice strain in determining physical properties.[9] More recently, three groups,[9–11] all demonstrated that the electromagnetic transport behavior of CMR manganite multilayers has been attributed to presence of lattice strain and disorder in epitaxial films. These results illustrated the importance of lattice strain and interfaces in determining physical properties of the oxide multilayers.

Trilayers consisting of AFM insulating manganite sandwiched by two FM metallic manganites are of particular interests because of their promising applications as all-manganite spin valve. Salafranca et al.[12] have found high values of tunneling magnetoresistance (TMR) in all-manganite trilayer $La_{2/3}Sr_{1/3}MnO_3$ (FM)/$Pr_{2/3}Ca_{1/3}MnO_3$ (AFM)/$La_{2/3}Sr_{1/3}MnO_3$ (FM). Here, antiferromagnetic $Pr_{2/3}Ca_{1/3}MnO_3$ spacer does not present phase separation. Sirena et al.[13] concluded that FM coupling of $La_{0.55}Sr_{0.45}MnO_3$ layers occurred across $La_{0.67}Ca_{0.33}MnO_3$ spacer up to room temperature in $La_{0.55}Sr_{0.45}MnO_3$/$La_{0.67}Ca_{0.33}MnO_3$/$La_{0.55}Sr_{0.45}MnO_3$ trilayers. The ground state of some manganites tends to present phase separation, typically involving FM metallic and AFM charge ordered (CO)/orbital ordered (OO) insulating clusters. The charge ordering phenomena has been usually observed particularly when the dopant concentration is close to the commensurate value in manganite system. However, the interface coupling of manganite multilayer is more complex especially when two competing ground states, the FM metallic state and the CO/OO insulating state, are present.[14]

In our earlier studies, we found experimental evidence on the existence of ferromagnetic cluster phase and the monotonic enhanced MR with decrease of temperature in

a)Electronic addresses: wanghaiou@hdu.edu.cn and tanweishi@njust.edu.cn

$Pr_{0.7}Sr_{0.3}MnO_3/La_{0.5}Ca_{0.5}MnO_3/Pr_{0.7}Sr_{0.3}MnO_3$ (PSMO/LCMO/PSMO) trilayers grown on MgO substrate.[15] This effect may have opportunities in practical device application. In these trilayered structures, half-doped LCMO served as AFM spacer, in which CO and phase separation were observed.[15] We noted also that PSMO/LCMO films did not show any improved physical properties. The circumstance of bilayer may probably be different from that of trilayer due to addition of another interface in FM/AFM/FM system, especially in all-manganite trilayer with half-doped manganite LCMO spacer. In order to study the structural dependence of magnetic and electrical transport properties of these trilayers, it is essential to characterize the strain according to in-plane and out-of-plane lattice parameters. Moreover, the unit cell volume of thin film and its distortions may not be the same as those of the corresponding bulk material. Volume expansion or contraction caused by stain can be stabilized by partial cation substitution[16] or oxygen nonstoichiometry. In the early years, Millis *et al.*,[17] and Rao *et al.*,[18] have studied the three-dimensional (3D) strain in single layer $La_{1-x}Ca_xMnO_3$ films. However, the effects of three-dimensional strain on physical properties by measuring the out-of-plane and in-plane lattice parameters have not been reported.

In this article, we synthesized trilayers consisting of two FM metal material PSMO (top and bottom layers) and one AFM insulator material LCMO (spacer layer) on (001)-oriented single crystal MgO substrate to investigate the evolution of 3D strain states, magnetism and electronic transport properties of epitaxial trilayers as a function of spacer thickness and lattice mismatch.

II. EXPERIMENT

Conventional solid-state reaction was applied to synthesize the PSMO and LCMO target using high-purity ($\geq 99.99\%$) raw powders of Pr_6O_{11}, $SrCO_3$, La_2O_3, $CaCO_3$, and MnO_2. La_2O_3 and Pr_6O_{11} was predried in air at $1000\,°C$ for $12\,h$. MnO_2 was precalcined at $1000\,°C$ for $20\,h$ to form Mn_3O_4. Stoichiometric raw powders of Pr_6O_{11}, $SrCO_3$, La_2O_3, $CaCO_3$, and Mn_3O_4 for $Pr_{0.7}Sr_{0.3}MnO_3$ and $La_{0.5}Ca_{0.5}MnO_3$ were mixed and thoroughly ground for a long time, then were pressed into disk-shaped pellets with the diameter of $10\,mm$. The pellets were first sintered at $1100\,°C$ for $12\,h$ in furnace and then were sintered at $1400\,°C$ for $12\,h$. Finally the products were cooled down to room temperature slowly.

PSMO/LCMO/PSMO trilayers were grown on (001)-oriented single crystal MgO using pulsed laser deposition. MgO substrate is cubic with lattice constant $a_{MgO} = 0.4217\,nm$. Phase purity in two targets was confirmed by powder x-ray diffraction patterns (not shown here). According to results from Rietveld refinements of powder x-ray diffraction patterns, the structures of PSMO and LCMO were regarded as pseudo-cubic ones with lattice parameter of $0.38744\,nm$ and $0.38223\,nm$, respectively. Moreover, PSMO buffer layer with the thickness of $5\,nm$ was grown on MgO substrate first to eliminate substrate-induced lattice strain of bottom PSMO sublayer. In the series of PSMO/LCMO/PSMO trilayers, the thickness of bottom and top PSMO layers was kept constant as $36\,nm$ while the thickness of LCMO spacer varied from

$6\,nm$ to $36\,nm$. The beam of KrF excimer laser ($\lambda = 248\,nm$) was focused on rotating target with energy density about $3\,J/cm^2$. Before deposition, MgO substrate was ultrasonic-cleaned with acetone, alcohol and de-ionized water in turn and the base pressure in the growth chamber was pumped to about 2×10^{-5} mbar. During deposition, the oxygen pressure was kept as 5×10^{-1} millibar, and substrate temperature was stabilized at $720\,°C$. The repetition rate of deposition was $2\,Hz$. The growth rates of PSMO and LCMO film were accurately calibrated so as to control the thickness of sublayers. All the samples were post-annealed in $1\,atm$ pure oxygen for half an hour and cooled down slowly in the same oxygen pressure. Wavelength dispersive x-ray spectroscopy (WDS) confirmed that the composition of the sublayer is the same as that of corresponding target within experimental error.

High-angle x-ray diffraction (HAXRD), asymmetric x-ray diffraction (AXRD), and low-angle x-ray reflection (LAXRR) have been used for the structural analysis of PSMO/LCMO/PSMO trilayers. In order to obviously observe distinct x-ray diffraction peaks, these experiments were performed at Synchrotron Radiation Facility with high resolution. HAXRD and AXRD experiments were carried out in beam line BL14B of Shanghai Synchrotron Radiation Facility (SSRF) with x-ray wavelength $0.12423\,nm$. LAXRR experiments were performed in beam line 1W1A of Beijing Synchrotron Radiation Facility (BSRF) with x-ray wavelength $0.15405\,nm$. The scattered intensity was recorded with NaI scintillation counter. The 3D strain states and in-plane and out-of-plane lattice parameters were measured directly using HAXRD and AXRD techniques. The transport properties have been measured with the conventional four-point probe method, applying the magnetic field parallel to current flow direction. Magnetic measurements were performed in superconducting quantum interference device magnetometer with magnetic field in sample plane.

III. RESULTS AND DISCUSSION

We have used HAXRD, LAXRR, and atomic force microscopy to characterize structure of trilayers. Fig. 1(a) shows the high resolution x-ray diffraction pattern of PSMO/LCMO ($t_{AFM} = 36\,nm$)/PSMO trilayer on (001) MgO substrate. Besides the reflection from the substrate of MgO and the (002) peaks of PSMO and LCMO, no other peak is visible, demonstrating that the as-grown films are of single phase and single orientation. Crystalline quality of films was analyzed using the measured full width at half maximum (FWHM) of the on axis rocking curves. The FWHM of (002) peak of trilayer is comparable to that of single crystal MgO substrate, indicating the high quality of epitaxial layer. Fig. 1(b) shows the θ-2θ x-ray scan pattern around the (103) reflection of the sample. In order to study the in-plane epitaxy of these samples on MgO substrates, we performed φ scan experiments of the sample around asymmetric (103) planes of trilayer. The scans of (103) PSMO and (103) LCMO reflections were carried out with the same starting φ azimuth. The reflection intensity from the asymmetric (103) planes of PSMO and LCMO is shown in Fig. 1(c). The presence of four symmetric peaks with 90° interval confirms the
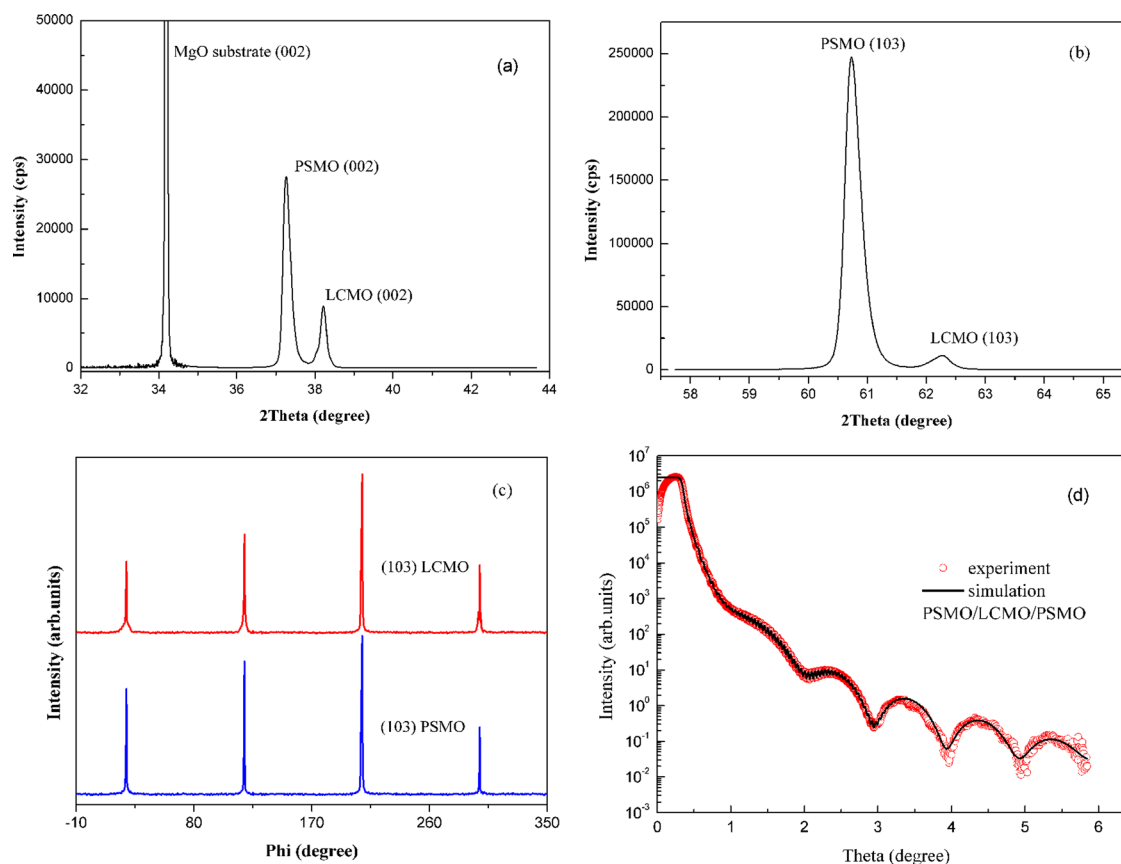
FIG. 1. Typical room temperature θ–2θ x-ray diffraction pattern of (a) around the (002) Bragg's diffraction peak and (b) around the (103) reflection of PSMO (36 nm)/LCMO (36 nm)/PSMO (36 nm)/MgO trilayer. (c) The φ scan patterns of (103) PSMO and (103) LCMO reflections of PSMO (36 nm)/LCMO (36 nm)/ PSMO(36 nm) starting from the same azimuth. (d) Experimental (open circle) and simulated (solid line) x-ray specular reflectivities of PSMO (36 nm)/LCMO (12 nm)/PSMO (36 nm) trilayer.

fourfold symmetry of pseudocubic perovskites. The reflection peaks of (103) PSMO and (103) LCMO appear at the same azimuth φ angle, representing an epitaxial relationship of PSMO [100]//LCMO [100]. The LAXRR and atomic force microscopy have been used to characterize the surface and interface structure of trilayers. The fitting results of LAXRR indicate rather smooth surface (root mean square surface roughness of about ~0.93 nm), negligible interlayer diffusion, and roughness at interface (interface structural characterization of the trilayers in detail will be reported elsewhere and are therefore discussed only briefly here). In atomic force microscopy image shown in Fig. 2, we can observe a very smooth surface with root mean square roughness about ~0.927 nm. This result is well consistent with above LAXRR fitting results within experimental error.

The evolution of in-plane and out-of-plane lattice parameters for two different sublayers (PSMO and LCMO) and associated lattice strain as a function of LCMO layer thickness are shown in Fig. 3. The strain relaxation processes are different for these two sublayers. For PSMO, as shown in Fig. 3(a), we can conclude that bottom and top PSMO layers have the same lattice parameter and both of them are fully out-of-plane strain-relaxed, and partially in-plane compressive strain-relaxed. For LCMO, the LCMO spacers (see Fig. 3(b)) are partially strained in average in reference to bulk LCMO. The lattice strain of LCMO begins to relax at very small thickness as mentioned above. As LCMO layer thickness increases, LCMO layer continues to relax gradually. Both in-plane and out-of-plane lattice parameters of LCMO sublayer tend to deviate away from initial value
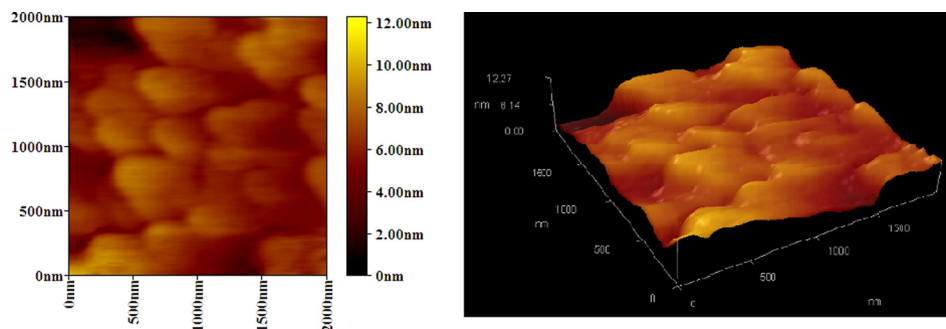

FIG. 2. Atomic force microscopy image of PSMO/LCMO/PSMO film on MgO substrate with LCMO thickness of 12 nm.
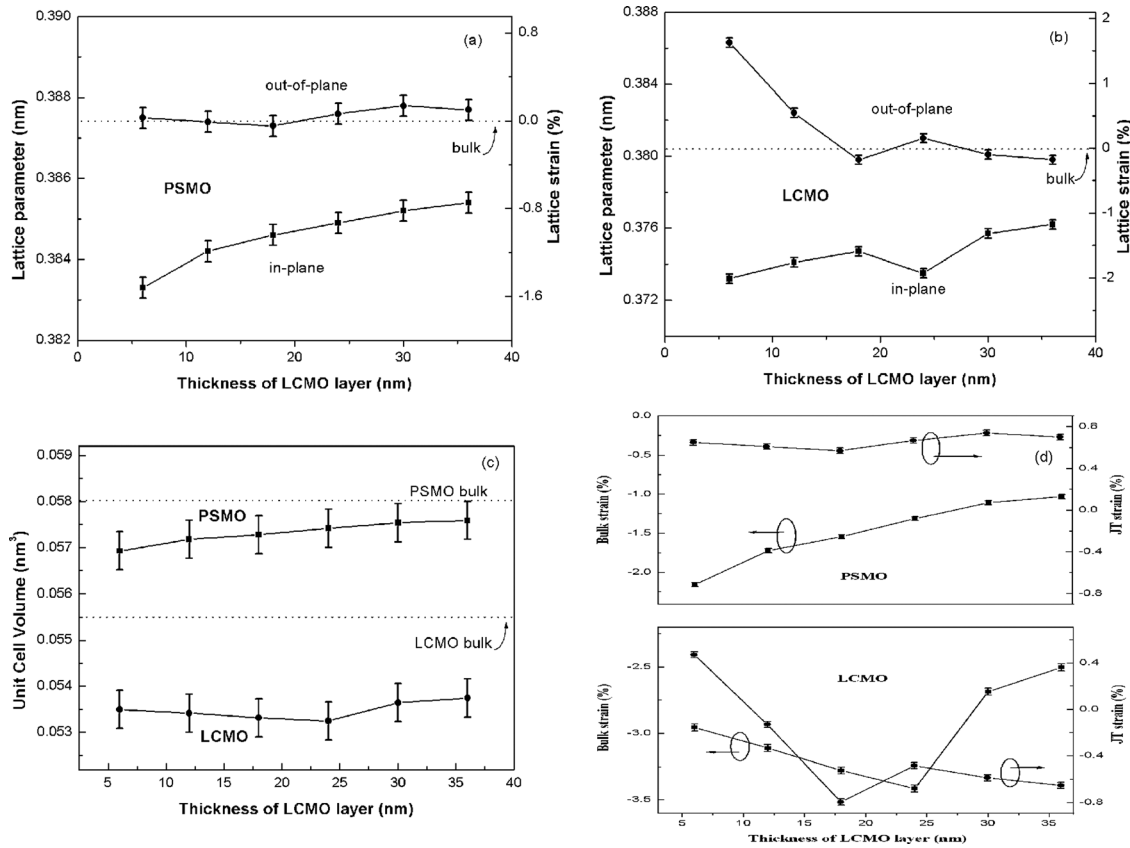
FIG. 3. LCMO thickness dependence of the measured out-of-plane (circles) and in-plane (square) lattice parameters and lattice strains of (a) PSMO sublayer and (b) LCMO sublayer. The lattice parameter of the corresponding bulk material measured from the target is indicated by the dotted lines. LCMO thickness dependence of (c) the perovskite unit cell volume and (d) bulk strain and JT strain of PSMO and LCMO sublayers. The cell volume of the bulk material is indicated by the dotted line.

towards the bulk value shown with dotted line in Fig. 3(b). Finally, out-of-plane lattice strain of LCMO is fully relaxed, but in-plane compressive bulk strain state remains. It should be pointed out that substrate-induced strain is likely to be fully relaxed at first growth stage due to the large lattice mismatch between PSMO buffer layer and MgO substrate. Here, strain in the trilayers stems mainly from interfacial lattice mismatch between PSMO and LCMO layer. For perovskite manganites, the intrinsic strain states are the bulk strain (ε_B) and the Jahn–Teller (JT) strain (ε_{JT}) as defined in Ref. 17. The bulk strain $\varepsilon_B = (\varepsilon_{xx} + \varepsilon_{yy} + \varepsilon_{zz})/3$ is associated with a hydrostatic volume distortion while the biaxial JT strain $\varepsilon_{JT} = (\varepsilon_{zz} - \varepsilon_{xx})/2$ corresponds to a tetragonal distortion of unit cell. Here, $\varepsilon_{xx} = \varepsilon_{yy}$ and ε_{zz} are the in-plane and

out-of-plane strain components, respectively. These strains have been calculated using the measured lattice parameters and listed in Table I. The JT strain, bulk strain, and the corresponding lattice cell volume exhibit a thickness-dependent variation with respect to LCMO layer thickness, as shown in Figs. 3(c) and 3(d). We note that the observed behavior in strain, particularly, the change of strain sign in LCMO layer shown in Fig. 3(b), probably results from different thermal expansion coefficient between MgO and PSMO and LCMO during films cooling from the high growth temperature. It could also be related to the oxygen stoichiometry in the films.

Temperature-dependent magnetization and resistivity of PSMO/LCMO/PSMO trilayers were measured to explore the

TABLE I. Measured electrical transport and magnetic data for trilayers and calculated Jahn–Teller and bulk strains for PSMO and LCMO thin films on (001) MgO substrate. The zero temperature resistivity intercept (ρ_0) gives an indication of the disorder in the film.

Thickness of AFM layer d_{LCMO} (nm)	ρ_0 (Ω·m)	T_{MI} (K)	T_C (K)	M_s (emu/g)	ε_{JT} (%)		ε_B (%)	
					PSMO	LCMO	PSMO	LCMO
6	1.27×10^{-3}	260	266	5.6	0.65	−0.47	−2.16	−2.96
12	3.51×10^{-3}	251	268	9.7	0.61	−0.13	−1.72	−3.11
18	2.46×10^{-2}	243	269	10.4	0.57	−0.79	−1.54	−3.28
24	3.32×10^{-2}	231	251	9.8	0.67	−0.48	−1.31	−3.41
30	10.86×10^{-2}	223	244	14.4	0.74	−0.59	−1.11	−2.69
36	15.74×10^{-2}	201	256	17.6	0.70	−0.65	−1.03	−2.50

233911-5   Wang et al.

J. Appl. Phys. 115, 233911 (2014)

effect of 3D strain states on magnetism and transport properties. Fig. 4(a) depicts the electrical transport properties of PSMO and LCMO ($d_{PSMO} = d_{LCMO} = 50$ nm) single layers without and with an applied magnetic field of 5 T. In Fig. 4(a), temperature-dependent resistivity of LCMO layer in zero Tesla field exhibits thermally activated behavior down to about 160 K and then an upturn can be clearly observed, indicating the presence of CO states. There also exists a characteristic temperature T* which is indicated with arrow in Fig. 4(a). The tendency of resistivity with temperature changes abruptly at temperature T*. When a magnetic field was applied, the resistivity of LCMO layer decreased and at about T* ∼ 100 K a metallic-like transport was observed. As for the PSMO layer, it undergoes a transition from insulator to metal at $T_{MI} \sim 256$ K. It should be pointed out that resistivity of LCMO layer was more than 100 times larger than that of PSMO layer, although they were depicted in Fig. 4(a) in the same scale for clarity. Fig. 4(b) shows the electrical transport properties of PSMO/LCMO/PSMO ($d_{LCMO} = 12$, 24, 36 nm) trilayers without and with an applied magnetic field of 5 T. From resistivity temperature-dependent curves, we can determine metal-insulator transition temperature T_{MI} of films, as listed in Table I. Interestingly, there exists a broad and weak peak at about 100 K at the left side of metal-insulation transition peak in the trilayer with LCMO thickness of 36 nm, which reflects the combined role of CO states and FM cluster percolation.

When a magnetic field is applied or LCMO layer thickness decreases, CO states will disappear and only MI transition peak can be discovered. In order to investigate the interlayer coupling, magnetic hysteresis loops of sample ($d_{LCMO} = 12$, 24, 36 nm) at 150 K were measured, as shown in Fig. 4(c). It is worth mentioning here that dependence of magnetic coercive field H_C on spacer thickness d_{LCMO} for the trilayers shows a sudden increase below $d_{LCMO} = 30$ nm, reaching a value of $\mu_0 H_C \sim 342.88$ Oe for $d_{LCMO} = 12$ nm. A similar enhancement of coercivity due to the formation of ferromagnetic clusters has been discussed by Ju and Sohn.[19] Thus, the enhancement of coercivity is probably associated to the formation of ferromagnetic clusters in inhomogeneous manganite films. Temperature-dependent magnetic and transport properties of PSMO/LCMO/PSMO trilayers have evidenced that a magnetic phase separation surely appears in the trilayers with thinner d_{LCMO} and transport properties are influenced by metallic ferromagnetic clusters percolation.[15] The field-cooled temperature-dependent magnetization of trilayers was measured with magnetic field of 1000 Oe, as shown in Fig. 4(d). All the samples showed a transition from paramagnetic (PM) to FM at T_C, which were listed in Table I. It is worthy to note that magnetization of films, except film with $d_{LCMO} = 12$ nm, start to increase with further decrease of temperature at about 100 K. This temperature is close to T* which is corresponding to the resistivity change shown in Fig. 4(a). The almost complete coincidence with T* further
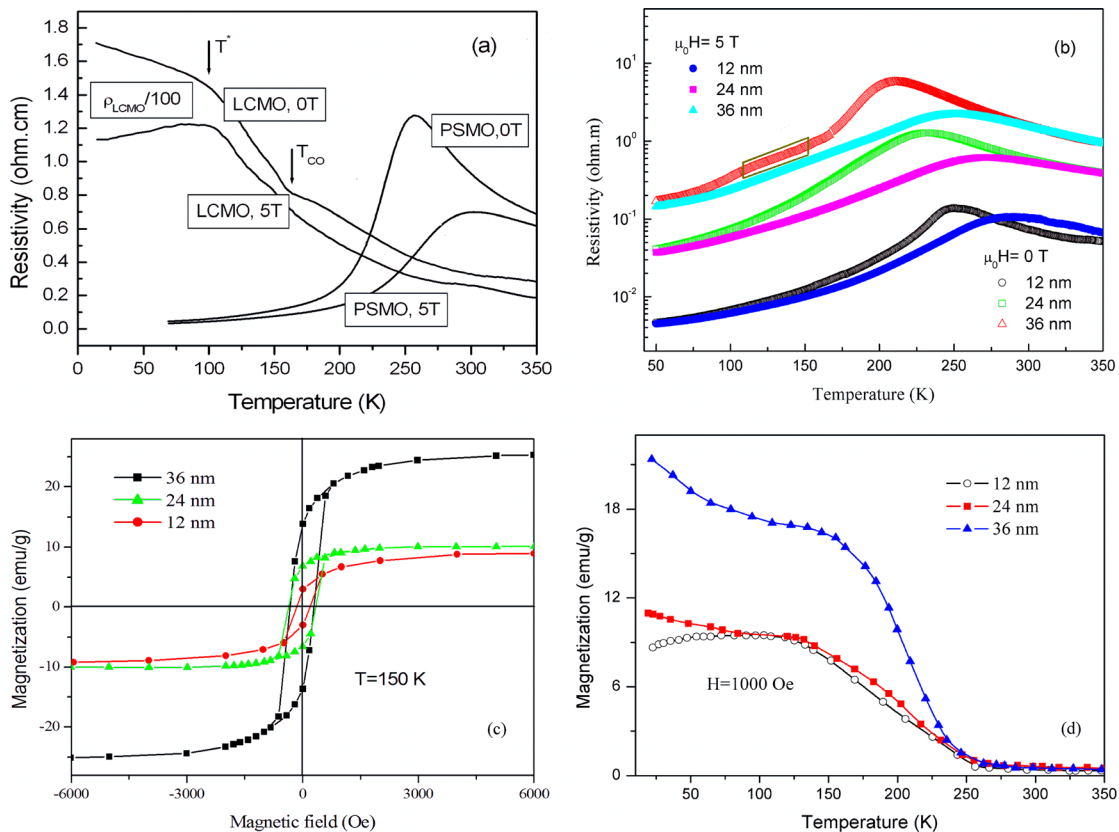

FIG. 4. Temperature dependence of resistivity of two reference single layers of PSMO and LCMO with thickness of 50 nm (a) and PSMO/LCMO/PSMO ($d_{LCMO} = 12$, 24, 36 nm) trilayers (b). Magnetic hysteresis loops of trilayers with $d_{LCMO} = 12$, 24, 36 nm after field-cooled in 1000 Oe. Temperature was fixed at 150 K during loop measurements (c). The temperature-dependent magnetization of trilayers with $d_{LCMO} = 12$, 24, 36 nm after field-cooled from room temperature to low temperature in 1000 Oe (d). All the measurements were performed by warming up in 1000 Oe.

[This article is copyrighted as indicated in the article. Reuse of AIP content is subject to the terms at: http://scitation.aip.org/termsconditions. Downloaded to] IP:
147.8.204.164 On: Tue, 03 Feb 2015 03:56:33

confirms the enhancement of FM fraction in phase-separated LCMO layer. However, undesirable magnetization decrease at temperature lower than $T^* \sim 100\,K$ occurs in trilayer with the spacer thickness of 12 nm, but the possible reason is still unclear.

When LCMO film was cooled from room temperature to low temperature, LCMO film first underwent a transition from PM insulation to FM metal, and then to a CO state accompanied with a transition from FM metal to AFM insulator at $T_{CO} \sim 160\,K$. The AFM and FM clusters coexist in LCMO film when temperature is lower than T_{CO}. The volume fraction of metallic FM clusters increases with further decrease of temperature and FM clusters start to percolate; therefore, resistivity of film starts to decrease at $T^* \sim 100\,K$, and a metallic-like transport is observed. The above mentioned mechanism of FM cluster percolation can be also further confirmed by M-T curve shown in Fig. 4(d). Because resistivity of LCMO is more than 100 times larger than that of PSMO, the total resistivity of PSMO/LCMO/PSMO (FM/AFM/FM system) is obviously influenced by LCMO. Therefore, we can propose reasonably that a large number of metallic FM clusters will exist on the interface between top PSMO and LCMO according to a simple parallel circuit model. The increase of magnetization with the LCMO layer thickness and the enhancement of H_C of the trilayer are associated with the CO state of the LCMO layer. The CO state may partially be responsible for the enhancement of ferromagnetism and the phase separation tendency in the trilayer structures.

Ferromagnetic Curie temperature (T_C), metal-insulator transition temperature (T_{MI}), the saturation magnetization (M_S) verus d_{LCMO} for all trilayers, and zero-temperature resistivity intercept ρ_0 have been obtained and listed in Table I along with the structural data. While T_{MI} of the films decreases monotonically with increasing d_{LCMO}, T_C does not obey a monotonic variation with d_{LCMO}, as shown in Fig. 5(a). Clearly, M_S increases gradually with increase of the LCMO-spacer-layer thickness and saturates for the film with $d_{LCMO} > 12\,nm$ with saturation value about $\sim 10\,emu/g$, but shows an upturn increase at $d_{LCMO} > 24\,nm$. This indicates a complex magnetic interaction in studied trilayers. Zero-temperature resistivity ρ_0 of the films decreases with decreasing d_{LCMO}, indicating reduction of short-range disorder in the film. While both transition temperatures and strain states exhibit strong thickness dependence as mentioned above, they seems not to show clear correlation with each other (see Figs. 5(b) and 5(c)). It is believed that lattice compression (negative ε_B) will reduce electron–phonon interactions and increase the electronic hopping amplitude by decreasing the Mn–O bondlength and increasing the Mn–O–Mn bond angle.[20,21] All these factors will lead to increasing T_C. In contrast, the Jahn–Teller distortion will lead to localization of electrons and thus reduce T_C. Therefore, the competition between bulk strain and JT strain play a vital role in electromagnetic transport properties of PSMO/LCMO/PSMO trilayers. For example, with decrease of LCMO layer thickness in PSMO/LCMO/PSMO trilayers, both PSMO and LCMO layers obey an increase trend
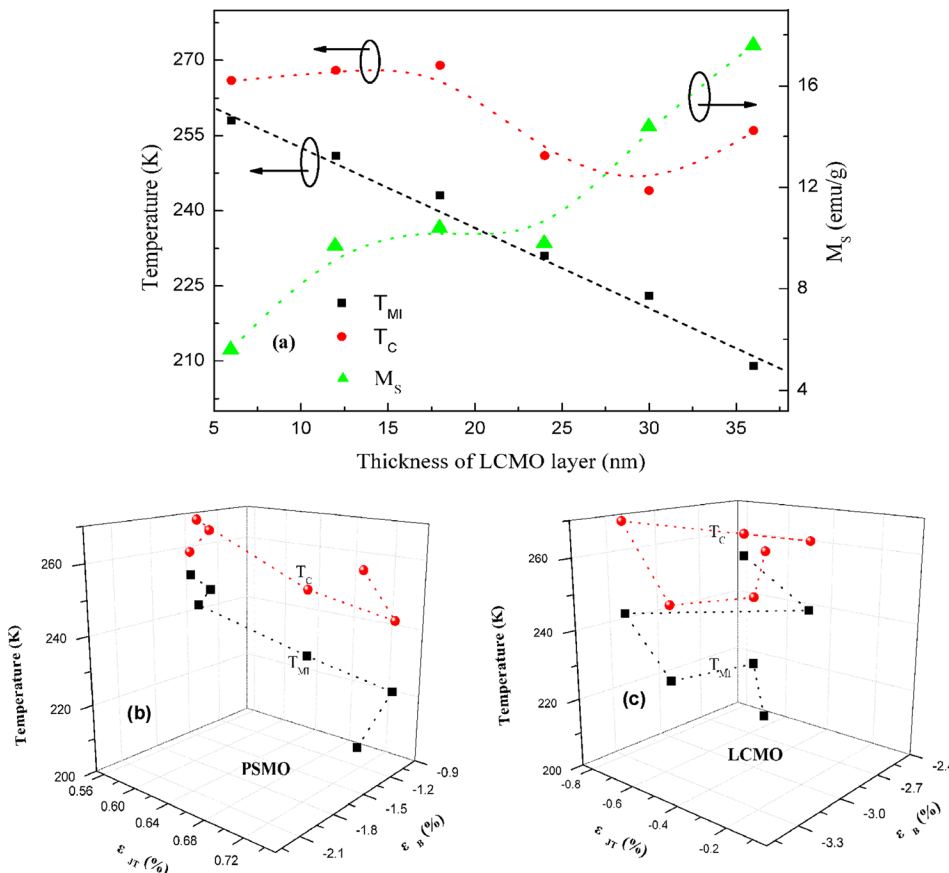

FIG. 5. LCMO layer thickness dependence of metal-insulator transition temperature T_{MI}, magnetic transition temperature T_C, and saturation magnetization M_S (a). T_C and T_{MI} of PSMO/LCMO/PSMO trilayers versus ε_{JT}, ε_B of PSMO layer (b) and LCMO layer (c). The dotted lines are drawn to guide the eye.

of compression bulk strain while JT strain decrease (see Fig. 4(d)), which lead to a monotonic T_{MI} increase together (see Figs. 5(a)–5(c)). This also proves a directly correlation between the three-dimensional strain states and T_{MI}. However, T_C does not comply with a systemic variation with respect to LCMO thickness and three-dimensional strain of PSMO and LCMO layer. The lack of correlation between the strain states and T_C shown here suggests that the Curie temperature is also influenced to a large extent by other factors, such as inhomogeneity and disorder in the film.

IV. CONCLUSIONS

In summary, we have studied the evolution of 3D strain states and magnetic and transport properties of epitaxial PSMO/LCMO/PSMO trilayer structures on MgO substrate as a function of LCMO layer thickness and lattice mismatch. We attributed the transport behavior to the CO state and 3D strain states induced by the lattice mismatch and strain relaxation at the interfaces. We showed that observed strain states exhibited a systematic change with respect to film thickness and the unit cell volume was not conserved. While electrical transition temperature showed strong dependence of LCMO thickness and clear correlation with strain states, magnetic transition temperature did not show clear correlation with LCMO thickness and strain states. Other key questions such as strain states at growth temperature and at T_C and other factors that control T_C still need to be addressed, but the 3D strain states presented here is an important first step towards elucidating the magnetic and electrical transport properties of CMR trilayers.

ACKNOWLEDGMENTS

[1]S. Jin, T. H. Tiefel, M. McCormack, R. A. Fastnacht, R. Ramesh, and L. H. Chen, Science **264**, 413 (1994).

[2]J. Z. Sun, W. J. Gallagher, P. R. Duncombe, L. Krusin-Elbaum, R. A. Altman, A. Gupta, Y. Lu, G. Q. Gong, and G. Xiao, Appl. Phys. Lett. **69**, 3266 (1996).

[3]C. Chappert, A. Fert, and V. D. F. Nguyen, Nat. Mater. **6**, 813 (2007).

[4]A. Sadoc, B. Mercey, C. Simon, D. Grebille, W. Prellier, and M. B. Lepetit, Phys. Rev. Lett. **104**, 046804 (2010).

[5]Y. Takamura, F. Yang, N. Kemik, E. Arenholz, M. D. Biegalski, and H. M. Christen, Phys. Rev. B. **80**, 180417(R) (2009).

[6]M. Egilmez, M. Abdelhadi, Z. Salman, K. H. Chow, and J. Jung, Appl. Phys. Lett. **95**, 112505 (2009).

[7]J. Garcia-Barriocanal, F. Y. Bruno, A. Rivera-Calzada, Z. Sefrioui, N. M. Nemes, M. G. Hernandez, J. R. Zuazo, G. R. Castro, M. Varela, S. J. Pennycook, C. Leon, and J. Santamaria, Adv. Mater. **22**, 627 (2010).

[8]F. Yang, N. Kemik, M. D. Biegalski, H. M. Christen, E. Arenholz, and Y. Takamura, Appl. Phys. Lett. **97**, 092503 (2010).

[9]Y. X. Han, W. B. Wu, G. S. Jiang, and C. F. Zhu, J. Appl. Phys. **111**, 066104 (2012).

[10]F. Cossu, U. Schwingenschlögl, G. Colizzi, A. Filippetti, and V. Fiorentini, Phys. Rev. B **87**, 214420 (2013).

[11]S. Dong, Q. F. Zhang, S. J. Yunoki, J. M. Liu, and E. Dagotto, Phys. Rev. B **86**, 205121 (2012).

[12]J. Salafranca, M. J. Calderón, and L. Brey, Phys. Rev. B **77**, 014441 (2008).

[13]M. Sirena, N. Haberkorn, L. B. Steren, and J. Guimpel, J. Appl. Phys. **93**, 6177 (2003).

[14]A. Moreo, S. Yunoki, and E. Dagotto, Science **283**, 2034 (1999).

[15]H. O. Wang, P. Dai, H. Liu, W. S. Tan, F. Xu, X. S. Wu, Q. J. Jia, G. J. Hu, and J. Gao, Int. J. Mod. Phys. B **26**, 1250132 (2012).

[16]R. A. Rao, Q. Gan, R. J. Cava, Y. Suzuki, S. C. Gausepohl, M. Lee, and C. B. Eom, Appl. Phys. Lett. **70**, 3035 (1997).

[17]A. J. Millis, T. Darling, and A. Migliori, J. Appl. Phys. **83**, 1588 (1998).

[18]R. A. Rao, D. Lavric, T. K. Nath, C. B. Eoma, L. Wu, and F. Tsui, Appl. Phys. Lett. **73**, 3294 (1998).

[19]H. L. Ju and H. Sohn, J. Magn. Magn. Mater. **167**, 200 (1997).

[20]H. Y. Hwang, T. T. M. Palstra, S.-W. Cheong, and B. Batlogg, Phys. Rev. B **52**, 15046 (1995).

[21]J. M. De Teresa, M. R. Ibarra, J. Blasco, J. Garcia, C. Marquina, P. A. Algarabel, Z. Arnold, K. Kamenev, C. Ritter, and R. von Helmolt, Phys. Rev. B **54**, 1187 (1996).